Journal of proteome research

pubs.acs.org/jpr

Article

Proteomic Analysis of Caco-2 Cells Disrupted by EcN 1917-Derived OMVs Reveals Molecular Information on Bacteria-Mediated Cancer Cell Migration

Ling Zhao, Mingxin Zhao, Xiankun Wang,* and Chenxi Jia*

Cite This: https://doi.org/10.1021/acs.jproteome.4c00176

Read Online

ACCESS | Metrics & More | Article Recommendations | Supporting Information

ABSTRACT: *Escherichia coli* Nissle 1917 (EcN 1917) exhibits distinct tumor-targeting activity, and early studies demonstrated that outer membrane vesicles (OMVs) mediate bacteria−host interactions. To decipher the molecular mechanism underlying the interaction between EcN 1917 and host cells via OMV-mediated communication, we investigated the phenotypic changes in Caco-2 cells perturbed by EcN 1917-derived OMVs and constructed proteomic maps of the EcN 1917-derived OMV components and OMV-perturbed host cells. Our findings revealed that the size of the EcN 1917-derived OMV proteome increased 4-fold. Treatment with EcN 1917-derived OMVs altered the proteomic and phosphoproteomic profiles of host cells. Importantly, for the first time, we found that treatment with EcN 1917-derived OMVs inhibited cancer cell migration by suppressing the expression of ANXA9. In addition, phosphoproteomic data suggested that the ErbB pathway may be involved in OMV-mediated cell migration. Taken together, our study provides valuable data for further investigations of OMV-mediated bacteria−host interactions and offers great insights into the underlying mechanism of probiotic-assisted colorectal cancer therapy.

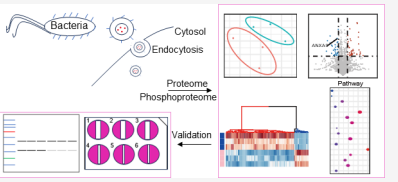

KEYWORDS: *host−bacteria interaction, Escherichia coli Nissle 1917, outer membrane vesicle, cancer cell migration, ANXA9*

INTRODUCTION

Probiotics are a group of microorganisms that contribute to regulating the gut microbiota and are widely used to prevent or treat gastrointestinal disorders and diseases, such as diarrhea, irritable bowel syndrome, and inflammatory bowel disease (IBD).[1] Probiotics help maintain human health through various mechanisms, including regulating immune function, producing organic acids or antimicrobial compounds, and interacting with other microbial communities.[2] In addition to preventing diseases related to digestive system disorders, probiotics can prevent colorectal cancer by altering the gut microbiota and potentially through immunomodulatory mechanisms.[3] The administration of the bacterium *Escherichia coli* Nissle 1917 (EcN 1917), a popular probiotic, effectively inhibits the growth of colorectal cancer in animal models.[4] EcN 1917 is a well-studied probiotic with multiple beneficial effects, including treating chronic inflammatory diseases and enhancing intestinal barrier function.[5,6] It has been recommended as a therapy for ulcerative colitis and shown to be as effective as mesalazine without affecting any pathogenic factors.[7] EcN 1917 has been demonstrated to inhibit pathogen adhesion, regulate immune responses,[8] and increase mucosal barrier integrity.[9] Additionally, EcN 1917 has shown tumor-targeting activity.[10] However, until now, no research has systematically reported how EcN 1917 impacts colorectal cancer cells or the underlying mechanism involved.

Recent studies have revealed that outer membrane vesicles (OMVs) are crucial for intercellular communication in the intestinal mucosal layer.[11] OMVs are secreted by Gram-negative bacteria and have a spherical double-layered phospholipid structure with diameters ranging from 20−250 nm.[12] As natural carriers of bacterial molecules, OMVs contain various bioactive molecules, including lipopolysaccharides, peptidoglycans, lipids, proteins, nucleic acids, and enzymes.[13] OMVs also function as a novel secretion system, allowing bacteria to transport active substances over long distances to various organs of the host in a protected environment without the need for direct cell-to-cell contact.[14] Thus, OMVs play crucial roles in communication between bacteria and host cells via intercellular communication, immune response regulation, and cell signaling.[14] OMVs are considered safer than live or attenuated bacteria because they are nonreplicative and only a small dosage is needed to achieve therapeutic effects.[15] Indeed, Bexsero, an engineered vaccine based on OMVs, is used clinically as a meningococcal B vaccine for children.[16] Importantly, OMVs play important roles in cancer therapy. For example, OMVs derived from *Escherichia coli* exert unique antitumor effects on mice with colon cancer through IFN-γ.[15] OMVs from *Salmonella typhimurium* have the ability to kill human colon, breast, and liver cancer cells.[17] The engineered

Received: March 6, 2024
Revised: May 25, 2024
Accepted: May 27, 2024

modification of bacterial OMVs provides a new tool for the application of bacteria in cancer therapy.[18] Although EcN 1917 exhibits remarkable tumor-targeting activity, the underlying mechanisms remain unclear. Herein, we speculated that EcN 1917 may functionally interact with host cells via OMV-mediated communication and that investigating the proteomes of both bacterial OMV cargos and OMV-perturbed host cells may provide molecular information.

To address these questions, we performed phenotypic screening on OMV-perturbed Caco-2 cells and observed that intestinal epithelial barrier function was enhanced and cell migration was inhibited. Proteomic analysis of the OMV cargo revealed 764 proteins with diverse biological functions and potential for bacteria−host interactions. Treatment with OMVs changed the architecture of the host cell proteome and phosphoproteome, including alterations in signaling pathways that participate in the regulation of cell migration, i.e., the ErbB, MAPK and cAMP pathways. Further validation experiments indicated that EcN 1917-released OMVs can inhibit cell migration by downregulating ANXA9. Overall, our study is the first to demonstrate that EcN 1917 affects the migration of host cells via OMV-mediated communication and provides a valuable resource for research on bacteria−host interactions and new insights for the application of probiotics and cancer therapy.

EXPERIMENTAL SECTION

Bacterial Strain and Growth Conditions

At a constant shaking rate of 200 rpm, EcN 1917 (O6:K5:H1, obtained from BeNa Culture Collection, BNCC361741) was cultivated in Luria−Bertani medium at 37 °C, composed of 1% peptone, 0.5% yeast extract, and 1% sodium chloride. The optical density at 600 nm was used to monitor and record the growth condition of EcN 1917.

Isolation of OMVs from EcN 1917

The bacterial culture in the logarithmic growth phase was centrifuged at 4 °C at 4,500 g for 25 min, and the supernatant was collected. A 0.22 μm membrane (Millipore) was used to filter the supernatant, eliminating any residual bacterial cells or cellular debris. The filtered bacterial supernatant was transferred to an ultracentrifuge tube and centrifuged using an OPTIMA XPN-100 ultracentrifuge (Beckman) at 150,000 g for 90 min to separate OMVs. After discarding the supernatant, the bottom precipitate was resuspended in PBS and then transferred to 1.5 mL centrifuge tubes. After resuspending in PBS, the samples are combined and then centrifuged using an OPTIMA MAX-XP ultracentrifuge (Beckman) at 150,000 g for 90 min to further isolate OMVs. After that, the supernatant was discarded and the bottom precipitate was resuspended in PBS. All these operations were conducted at low temperature or on ice. OMVs were stored at 4 °C for short-term use or at −80 °C for long-term storage as needed.

Nanoparticle Tracking Analysis (NTA)

The concentration and size distribution of the isolated OMVs were determined using the ZetaView PMX110 particle matrix by applying laser light to the suspension of nanoparticles and detecting the scattered light. The OMVs were diluted with PBS to a concentration of 1×10^7 particles/mL to 1×10^9 particles/mL for NTA measurement.

Transmission Electron Microscopy (TEM)

A copper grid was filled with 10 μL of OMVs solution, which was left to incubate at room temperature for 10 min. Afterward, the superfluous liquid was eliminated by rinsing with sterile distilled water and absorbing with filter paper. Subsequently, 10 μL of 2% uranyl acetate was applied to the copper grid for negative staining for 1 min, and the excess fluid was removed with filter paper. The grid was then dried under an incandescent lamp for 2 min and observed using a transmission electron microscope at 80 kV.

In-Gel Digestion of OMV Proteins

The in-gel enzymatic digestion method was employed to prepare OMVs protein samples for LC-MS analysis, according to a previous report.[19] Briefly, the EcN 1917 OMV samples were mixed with lysis buffer (1% SDS, 1% protein inhibitor) and sonicated, followed by boiling at 70 °C for 10 min. After centrifugation at 14,000 g for 10 min, the supernatant was collected, and the BCA protein assay kit was used to quantify the protein concentration. Subsequently, 10 μg protein were applied to SDS-PAGE gel separation, followed by staining with Coomassie's brilliant blue. The stained area in the gels were cut into 1 mm^3 pieces and placed a tube. After rinsing and destaining, 100% ACN was applied to dehydrate the gel particles, then 10 mM dithiothreitol (DTT) in 50 mM NH_4HCO_3 was used to reduce disulfide bonds for 30 min at 56 °C, and then 30 mM iodoacetamide (IAA) was added and incubated for 20 min in a dark chamber. After wash, trypsin solution (1:50, w/w, Promega) was added to completely envelop the gel particles for overnight digestion at 37 °C. The tryptic peptides were extracted from gels with 50% ACN/0.1% formic acid (FA) for three times. The combined gel extraction was dried in a vacuum concentrator and resuspended water/0.1% FA for LC-MS/MS analysis.

Cell Culture and OMV Treatment

The human colon adenocarcinoma cell line, Caco-2 (ATCC HTB-37, Shanghai Jinyuan Biotechnology) was cultured in RPMI-1640 medium (Gibco) supplemented with 10% fetal bovine serum (FBS), 100 mg/mL streptomycin, and 100 IU/mL penicillin in a humidified incubator (Thermo Fisher) with 5% CO_2 and 37 °C. When the cells were >70−80% confluent, the certain amount of OMVs containing 100 μg proteins were added into cells to a final concentration of 10 μg/mL OMV proteins in the mixture, followed by culture for additional 24 h. Finally, the cells were subjected to phenotypic assay or collected for preparation of proteins.

Confocal Microscopy

To obtain OMVs labeled with DiO (Beyotime Biotechnology C1993S), the extracted OMVs were incubated with the lipophilic dye DiO at room temperature under light-shielded conditions for 25 min, followed by removal of excess dye through ultracentrifugation. The OMVs labeled with DiO were then coincubated with Caco-2 cells for 2 h. After washing the cells with PBS for three times, Hoechst dye was applied to stain the nuclei for 10 min. Subsequently, the cells were washed with PBS for three times again and subjected to confocal laser scanning microscopy (LSM880 ELYRA, Carl Zeiss) using a 63 × 1.4 oil immersion lens. The images were acquired to visualize the internalization of OMVs within the cells.

https://doi.org/10.1021/acs.jproteome.4c00176
J. Proteome Res. XXXX, XXX, XXX−XXX

Lactate Dehydrogenase (LDH) Assay

Caco-2 cells were seeded in 96-well plates with 1×10^4 cells per well, and the culture medium was discarded. After washing once with PBS, the cells were cultured with a low-serum culture medium containing 1% serum. The cell culture wells were divided into three groups, including cell-free, untreated cell group, and OMV-treated cell group. In the OMV-treated cell group, a dose gradient of OMVs, e.g., 1, 2, and 5 μg, were added respectively to result in final concentrations of 5, 10, and 25 μg/mL, and 5 replicates were set for each dose. After continuously culturing for 24 h, 120 μL of supernatant was collected from each well and transferred into a fresh 96-well plate, followed by measuring the Multifunctional microplate reader system (BioTek) in accordance.

Cell Migration Assay

A monolayer of cells was formed by the seeding of Caco-2 or NCM 460 cells into a six-well plate, which was then cultured in the correct medium and conditions to reach a suitable density. Using a 10 μL pipet tip, a uniform wound area was created by lightly scratching a line on the cell monolayer. The experiment was divided into a control group and an OMVs group. In the OMVs group, 10 μg/mL of OMVs were added to each well, while the same volume of PBS was added to the control group. After incubation for 24 h, the culture medium was discarded and the cells were washed twice with PBS, and then fresh PBS was added to maintain cell viability. An inverted microscope (Nikon) was utilized to capture images of the scratch region, which were then subjected to ImageJ image processing software analysis. The initial area of the scratch and the area of the scratch after incubation were quantified by ImageJ. The threshold was adjusted so that the mask filled in the scratch, and then Magic Wand tool was used to select the scratch, establish a selection area, and measure the actual scratch area. Cell migration was calculated as [(initial scratched area − remaining scratched area at 24 h incubation)/initial scratched area] × 100%.

Epithelial Cell Permeability Measurement

Caco-2 cells were seeded on a 0.44 μm polyester membrane of Transwell (Thermo Fisher) at a density of 2.5×10^5 to simulate a monolayer cell model of the intestinal epithelium over the course of 21 days. After culture for 21 days, 100 μg/mL of fluorescein isothiocyanate−dextran (FD4) (Sigma-Aldrich) was added into the upper chamber of Transwell. The cells were then incubated for 2 h in the medium containing FD4, allowing FD4 to penetrate the cell barrier. The lower Transwell chambers were placed in Multifunctional microplate reader system (BioTek) to measure the FD4 fluorescence intensity with an excitation wavelength of 485 nm and an emission wavelength of 520 nm. This measurement reflects the movement of FD4 from the upper cell monolayer to the lower chamber and is used to evaluate cell barrier permeability.[20]

Sample Preparation for Proteomic and Phosphoproteomic Analysis of Caco-2 Cells

A previously reported strategy of filter-assisted sample preparation (FASP)[21] was used to prepare the protein samples. Briefly, the cell was treated with a SDT lysis buffer composed of 4% SDS, 100 mM Tris/HCl (pH 7.6), 0.1 M DTT, 1% protease inhibitors, and 1% phosphatase inhibitors. After that, 80 μg of protein sample was added into a 10-kDa molecular weight cutoff filter (Millipore), and solvent exchange was performed by centrifuge for twice using UA (8 M urea in 0.1 M Tris/HCl pH 8.5) to remove SDS, and then 50 mM IAA (in UA) had been added, followed by incubation in the dark for 20 min. The filter was washed twice with UB (8 M urea in 0.1 M Tris/HCl pH 8.0). To bring the urea concentration below 1 M, 50 mM NH_4HCO_3 was added and trypsin digestion (1:50, w/w) was conducted overnight. The supernatant was collected after centrifugation, and the samples were dried and resuspended in water/0.1% FA for LC-MS analysis.

The phosphopeptide enrichment was performed according to a previous published protocol.[22] Briefly, 1 mg of tryptic digest resulting from FASP as described above was resuspended in a phosphopeptide binding buffer composed of 70% ACN, 5% TFA, and 8.3% lactic acid (LA) and loaded on TiO_2 beads. Then, binding buffer, wash buffer 1 (30% ACN, 0.5% TFA), and wash buffer 2 (80% ACN, 0.5% TFA) were sequentially added twice, with vertical mixing for 10 min and centrifugation at 3,000 g for 1 min. The phosphopeptides were eluted twice with an appropriate elution buffer (40% ACN, 15% NH_4OH), followed by centrifugation at 3,000 g for 1 min and dried by vacuum centrifuge.

LC-MS/MS Analysis

For proteomic analysis, peptides were analyzed using Orbitrap Fusion (Thermo Scientific) coupled to an EASY-nano-LC 1200 system (Thermo Scientific). The tryptic peptides were redissolved in solvent A (solvent A, water/0.1% FA); solvent B, 95% ACN/0.1% FA) and loaded onto a homemade trap column (100 μm × 2 cm; particle size, 3 μm; pore size, 120 Å; SunChrom) at a flow rate of 10 μL/min. The sample was subsequently separated with a homemade analytical column at a flow rate of 600 nL/min (150 μm × 12 cm; particle size, 1.9 μm; pore size, 120 Å; SunChrom). The electrospray voltage of 2.3 kV versus the inlet of the mass spectrometer was used. Survey full scans were acquired from 300 to 1400 m/z at a resolution of 120,000 and the maximum injection time was set to 100 ms or an automatic gain control (AGC) target of $5e^5$. Data-dependent acquisition with Top20 were used per cycle with dynamic exclusion time of 18 s. The activation type was higher-energy collision dissociation (HCD) with a normalized collision energy of 35% and MS/MS scan resolution was 60,000 and the maximum injection time was set to 118 ms or an AGC target of $5e^4$.

For phosphoproteomic analysis, the LC-MS/MS analysis was carried out on an Orbitrap Q Exactive HF mass spectrometer (Thermo Fisher Scientific) connected with an EASY-nLC 1200 nanohigh-performance LC system (Thermo Fisher Scientific). The sample loading, LC gradient and acquisition mode are the same as described above. The parameters of mass spectrometry include: spray voltage of 2.3 kV; resolving power of 120,000 at full-scan mode; 15,000 at MS/MS mode; normalized collision energy of 28%; automatic gain control targets of $3e^6$ ions for full scans and $2e^4$ for MS/MS scans; the maximum injection time of 80 ms for full scans and 22 ms for MS/MS scans; and dynamic exclusion was used for 12 s.

Western Blotting

The total cell lysates were extracted using SDT lysis buffer. A 10% SDS-PAGE gel was employed to separate 10 μg of protein samples, which had been mixed with SDS-PAGE sample buffer. A Bio-Rad Mini Transblot apparatus was employed to transfer the proteins to an immunoblot NC membrane. At room temperature for 1 h, PBS containing 0.05% Tween-20 was used to block the membrane with 5% nonfat milk. Afterward, the

https://doi.org/10.1021/acs.jproteome.4c00176
J. Proteome Res. XXXX, XXX, XXX−XXX

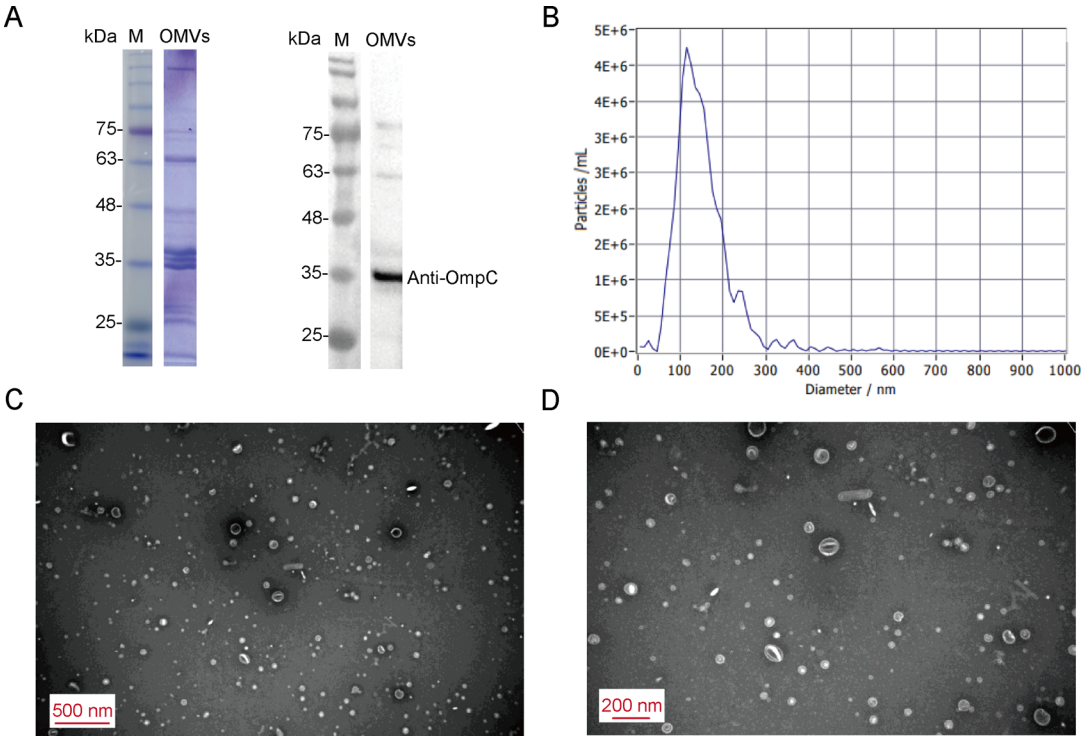

Figure 1. Characterization of EcN 1917-derived OMVs. (A) SDS-PAGE analysis (left) and Western blot (right) of EcN 1917-derived OMVs. (B) Nanoparticle tracking assay showing the size and density distribution, and (C, D) transmission electron micrographs of EcN 1917-derived OMVs.

blot was incubated for an entire night at 4 °C with primary rabbit antibodies against OmpC (Abebio, PA91378EC), ANXA9 (Abcam, ab166621), and α-tubulin (Servicebio, GB15201). Subsequent incubation was performed using secondary antibodies, peroxidase-conjugated goat antirabbit IgG (ZSGB-BIO, ZB-2301) at room temperature for 2 h. A chemiluminescence technique was employed to visualize the protein bands on 4800 Multi (Tanon).

Quantitative PCR

An RNA extraction kit (Transgene Biotech) was employed to extract total RNA from Caco-2 cells, and then 500 ng of total RNA was synthesized from cDNA using the PrimeScript RT kit (Takara). ANXA9 and α-tubulin primers were synthesized by Qingke Biotech (Table S1). Real-time PCR was performed using SYBR Green Master Mix (Toyobo) on the qTOWER system. The ΔΔCT method was employed to analyze the initial data, with α-tubulin serving as an internal regulator to normalize gene expression.

ANXA9-siRNA Transfection and ANXA9 Overexpression

For siRNA-mediated gene silencing, cells were transfected with 50 nM siRNAs using lipofectamin 2000 (Invitrogen) according to the product manual. To rule out potential off-target effects of siRNAs, two pairs of siRNAs for ANXA9 were designed. The sequences for siRNAs are listed in (Table S2).

The pcDNA3.1-Flag-ANXA9 plasmid with the ANXA9 protein DNA sequence (NM_003568.3, GenBank) was engineered. A Flag tag was added at the N-terminus to improve protein recognition and purification, and a Kozak sequence was included to enhance translation efficiency. The entire sequence was then cloned into the pcDNA3.1(+) vector at the *Hin*dIII and *Kpn*I restriction sites. The sequence was synthesized by Beijing Tsingke Biotech Co., Ltd. For overexpression of ANXA9 in cells, 2 μg of plasmid pcDNA3.1-Flag-ANXA9 was added into cells using 2.0 μL Neofect (Neo-biotech).

Mass Spectrometry Data Analysis

The proteomic search engine MaxQuant v2.2.0.0[23] was used for processing the.RAW data against database of the complete *E. coli* (UP000011176) protein sequence library within the UniProtKB database (comprising 4530 curated proteins, downloaded as of October 2022) or the complete human (UP000005640) proteome database (comprising 20426 curated proteins, downloaded as of October 2022). Parameter settings included: label-free quantification, trypsin for enzymatic cleavage, carbamidomethylation (C) for fixed modification, oxidation (M) for variable modification, 2 missed cleavages, and controlled the false discovery rate (FDR) to below 1% during identification. The match between runs function was enabled. A protein identification required at least two unique peptides. For phosphoproteomic analysis, phosphorylation (STY) was set as a variable modification. Phosphosite probability cutoff was set as 0.75. The identified proteins or phosphopeptides were filtered by the criteria of being at least 60% valid values in at least one group. Protein missing values were imputed by 0.1 multiples the minimum value in all groups. Because proteomic analysis was performed on Orbi-Ion trap mode, mass tolerance of precursors and fragments were set to 20 ppm and 0.5 Da, respectively; and 20 ppm and 0.02 Da were used for phosphoproteomic analysis due to Orbi−Orbi mode. Pearson correlation analysis was performed using the cor function from the corrplot package in R. The parameter was set to "pearson", and then the correlation matrix was plotted using the corrplot function. For PCA analysis, dimensionality reduction analysis was performed using the prcomp function in R, and then the result was visualized using the ggbiplot package.

https://doi.org/10.1021/acs.jproteome.4c00176
J. Proteome Res. XXXX, XXX, XXX−XXX

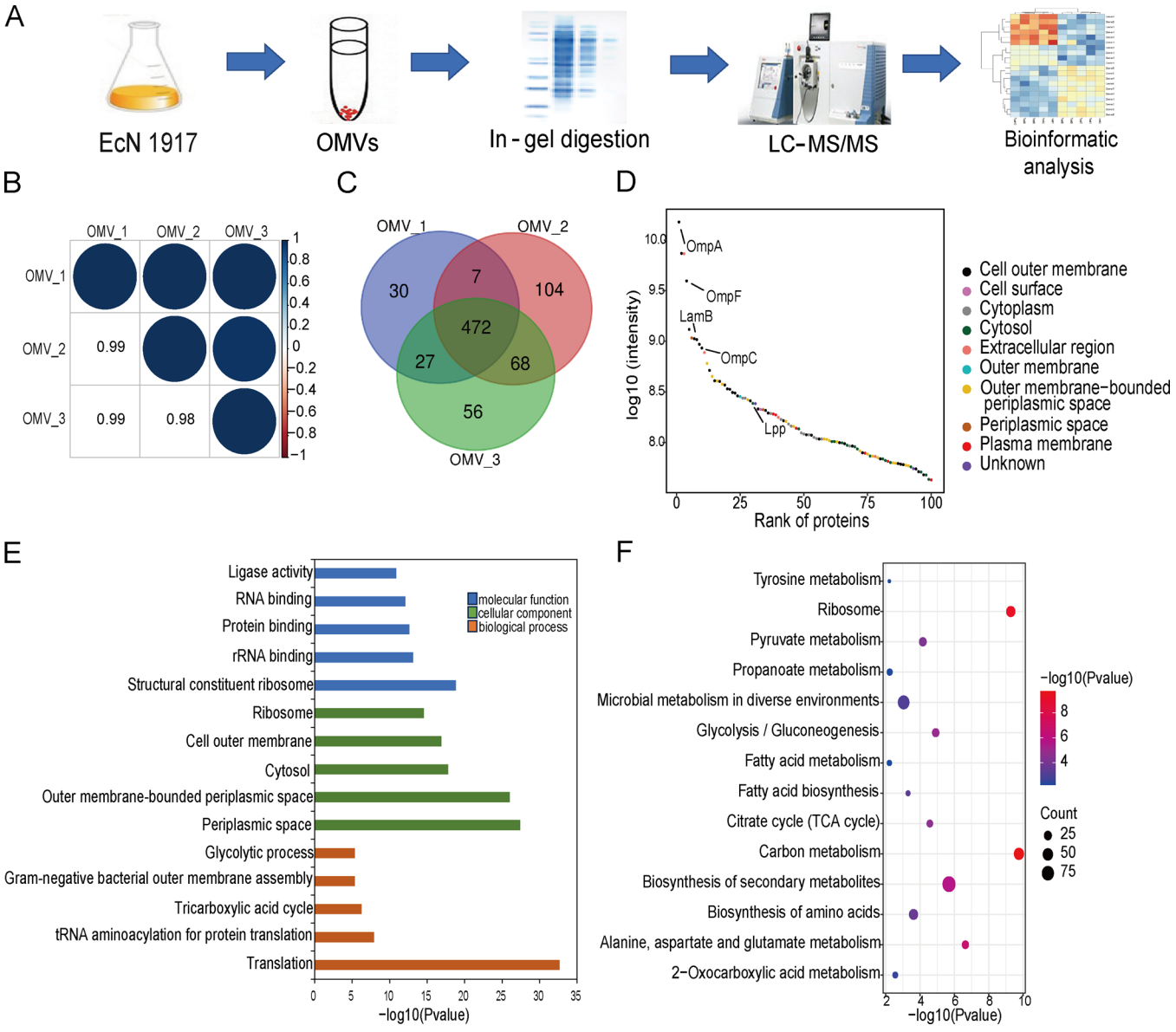

Figure 2. Identification of the EcN 1917-derived OMVs proteome cargos. (A) Workflow for proteomic analysis of the OMV cargos. (B) Pearson correlation of the three biological replicates. (C) Venn diagram showing the number of identified proteins in each replicate. (D) Ranking plot of the top 100 abundant identified proteins with annotation of subcellular localization. The classical OMV marker proteins, such as LamB, OmpC, OmpF, Lpp, and OmpA are highlighted. (E) GO enrichment and (F) KEGG enrichment of the identified proteins. GO, $p < 0.05$; KEGG, $p < 0.01$.

Bioinformatics Analysis

We used the DAVID database[24] for gene ontology (GO) functional enrichment analysis. Pathway analysis was performed using KEGG database. IPA was used to analyze protein−protein interaction networks and signaling pathways. Furthermore, we utilized the SMART database[25] to analyze the enrichment of functional domains of differentially expressed proteins, and visualized the results using iTOL. MotifR algorithm[26] was used to analyze the motif features of the modification sites. Protein−protein interaction analysis was performed on the differentially expressed proteins using STRING analysis, and the exported data was then submitted into Cytoscape for further analysis with MCODE plugin.

RESULTS

Characterization of EcN 1917-Derived OMVs and Quality Control

OMVs derived from EcN 1917 were prepared using an ultracentrifugation-based strategy. The quality control was determined by characterizing the protein markers on OMVs as well as the shape and particle size of the OMVs. SDS−PAGE revealed the presence of abundant proteins in OMVs, and Western blotting confirmed the presence of OmpC, a protein marker of OMVs (Figure 1A). Nanoparticle tracking analysis revealed that the size distribution of the OMVs ranged from 20−250 nm, with an average diameter of 149.4 nm (Figure 1B), which was consistent with previous reports.[12] TEM revealed that the OMVs had spherical structures (Figure 1C,D). These results demonstrated the reliable quality of the

https://doi.org/10.1021/acs.jproteome.4c00176
J. Proteome Res. XXXX, XXX, XXX−XXX

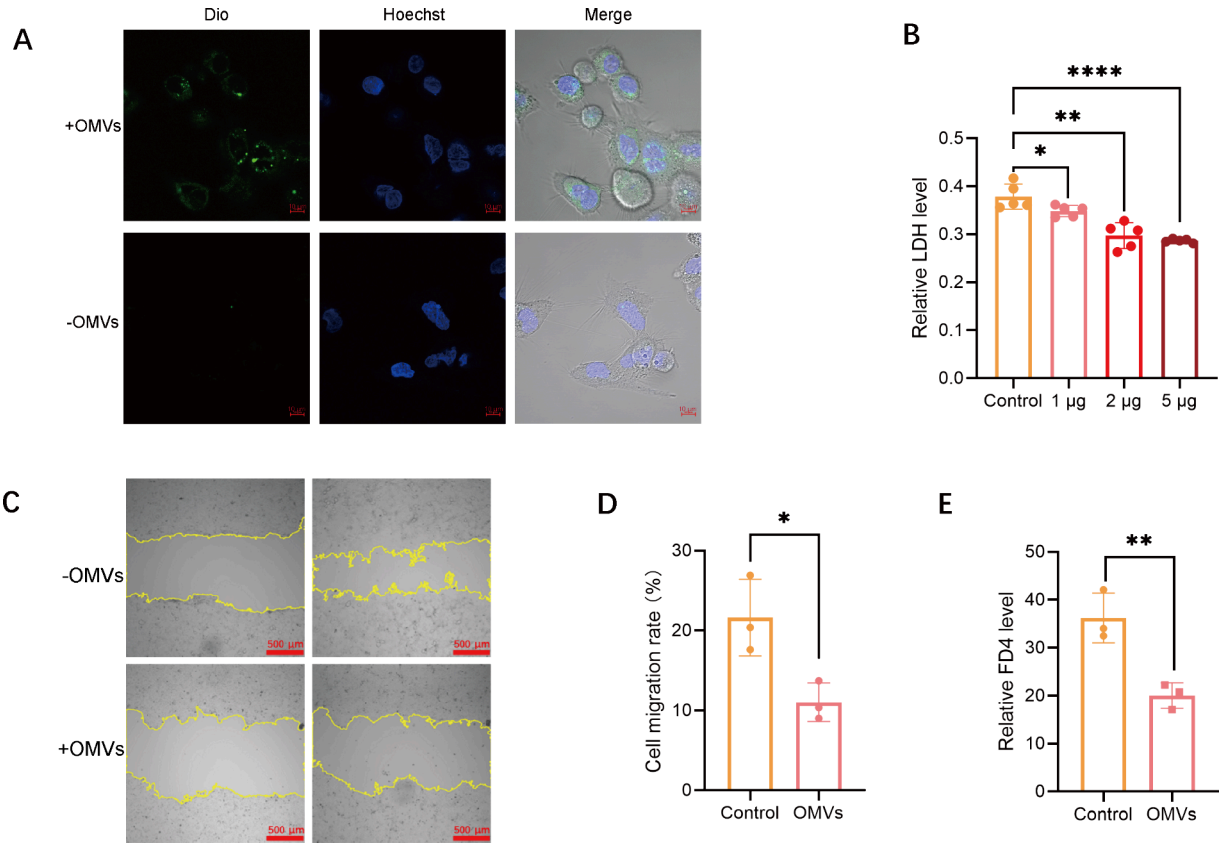

Figure 3. Internalization of EcN 1917-derived OMVs by Caco-2 cells and the cellular phenotypic changes. (A) Confocal microscope image of Caco-2 cells stained with Hoechst (blue signal) for uptake and internalization of unstained or DiO-labeled OMVs (green signal). (B) Lactate dehydrogenase activity in the cell culture supernatant after exposure to different concentrations of EcN 1917-derived OMVs for 24 h. (C, D) Effects of EcN 1917-derived OMVs on cell migration, measured by wound healing assay, with cell migration area assessed after 24 h, and (E) on cell permeability. Three biological replicates. Unpaired two-tailed Student's *t* test. $*p < 0.05$, $**p < 0.01$, $***p < 0.001$. Mean ± SD.

EcN 1917-derived OMVs that we obtained for subsequent experiments.

EcN 1917-Derived OMVs Carry Diverse Functional Protein Cargos

To determine the detailed proteome components of OMVs, especially those showing potential functions in host cell interactions, we conducted LC−MS/MS proteomic analysis using a streamlined workflow (Figure 2A). The Pearson correlation coefficient of the three biological replicates was >0.9 (Figure 2B), indicating the high reproducibility of the proteomic data. A total of 764 proteins were identified, which was approximately four times greater than the 189 proteins previously identified in the EcN 1917-derived OMV proteome (152 proteins were coidentified in our study);[27] thus, our data greatly expanded the EcN 1917-derived OMV protein database. Among these proteins, 472 were found in all three biological replicates (Figure 2C, Data file S1) and thus were selected for further analysis. Many proteins residing on the bacterial outer membrane were detected; these proteins contribute to bacteria−host interactions and are critical for the probiotic function of EcN 1917. For example, flagellar proteins (flgC, flgE, and flgK) participate in gut adhesion and colonization, and many proteins (FecA and FhuA) related to transport activities play roles in bacterial survival in the host ecological niche. Other compounds exhibited antimicrobial activity, e.g., mltA and mltC, and modulated host immunity, e.g., OmpA, OmpC and OmpF. These diverse probiotic-related proteins suggested that the EcN 1917 OMVs contain proteins that can influence host cells. The abundance of the top 100 proteins was plotted, and the proteins were distributed in different subcellular components of the bacteria (Figure 2D, Data file S2), suggesting diverse origins of the cargo proteins in OMVs. GO enrichment analysis indicated that the 472 proteins were mainly distributed in the cytoplasm, outer membrane, and periplasm and play important roles in multiple biological processes, including protein translation, the tricarboxylic acid cycle, Gram-negative bacterial outer membrane assembly, and glycolysis (Figure 2E). Additionally, the proteins exhibited molecular functions such as protein binding, RNA binding, and ligase activity. KEGG analysis revealed that multiple pathways, such as metabolic pathways, the TCA cycle, and the biosynthesis of secondary metabolites, were enriched (Figure 2F). Therefore, proteomic analysis of EcN 1917-derived OMVs revealed diverse protein cargos with potential involvement in host cell interactions.

EcN 1917-Derived OMVs Alter Multiple Phenotypes of Host Cells

Inspired by the finding that EcN 1917-derived OMVs contain abundant host cell-interacting proteins, we sought to confirm whether OMVs could be internalized by Caco-2 cells. The cells were coincubated with OMVs labeled with the green fluorescent lipophilic compound DiO. The cell nuclei were then labeled with Hoechst, followed by fluorescence signal detection. The presence of EcN 1917 OMVs in the cytoplasm

https://doi.org/10.1021/acs.jproteome.4c00176
J. Proteome Res. XXXX, XXX, XXX−XXX

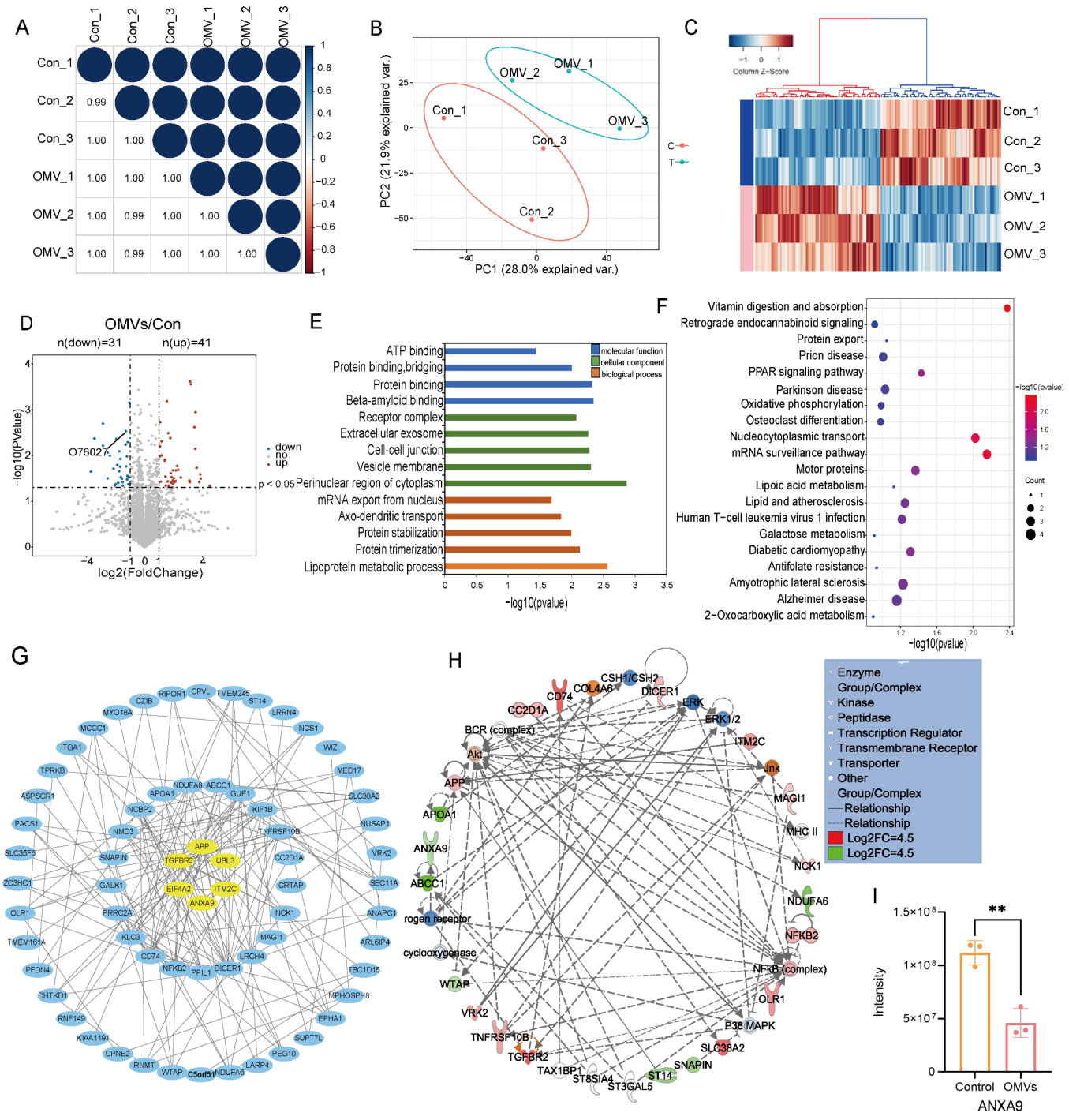

Figure 4. Proteomic analysis of Caco-2 cells perturbed by EcN 1917-derived OMVs. (A) Pearson correlation analysis of all proteomic data. (B) PCA plot of the proteomic data in OMV-treated cells (OMV) and OMV-free cells (Con). (C) Heat map and (D) volcano plot of differentially expressed proteins in OMV-treated cells compared to OMV-free cells. Differentially expressed proteins are determined by fold change >2 or <0.5 and $p < 0.05$. (E) GO and KEGG (F) enrichment of differentially expressed proteins. GO, $p < 0.05$; KEGG, $p < 0.01$. (G) String interaction analysis with a combined score >0.4, and (H) protein−protein interaction network analysis of differentially expressed proteins. (I) Bar graph showing the MS intensities of ANXA9 protein in Caco-2 cells after OMV treatment. Unpaired two-tailed Student's t test. *$p < 0.05$, **$p < 0.01$. Mean ± SD.

of the cells indicated the internalization of these vesicles by Caco-2 cells (Figure 3A).

We next conducted a series of phenotypic experiments, including assays of cytotoxicity, cell migration, and epithelial cell permeability, to investigate the possible effects of EcN 1917-derived OMVs on host cells. First, Caco-2 cells were treated with EcN 1917-derived OMVs at increasing concentrations, and then a cytotoxicity assay was performed. A decrease in cell membrane integrity caused the release of the intracellular enzyme LDH from the cells to the culture medium, which was detected as an indicator of cytotoxicity.[28] A marked decrease in LDH release was observed in the OMV-treated group (Figure 3B), suggesting that the addition of EcN 1917-derived OMVs prevented cell toxicity. Second, a wound

https://doi.org/10.1021/acs.jproteome.4c00176
J. Proteome Res. XXXX, XXX, XXX−XXX

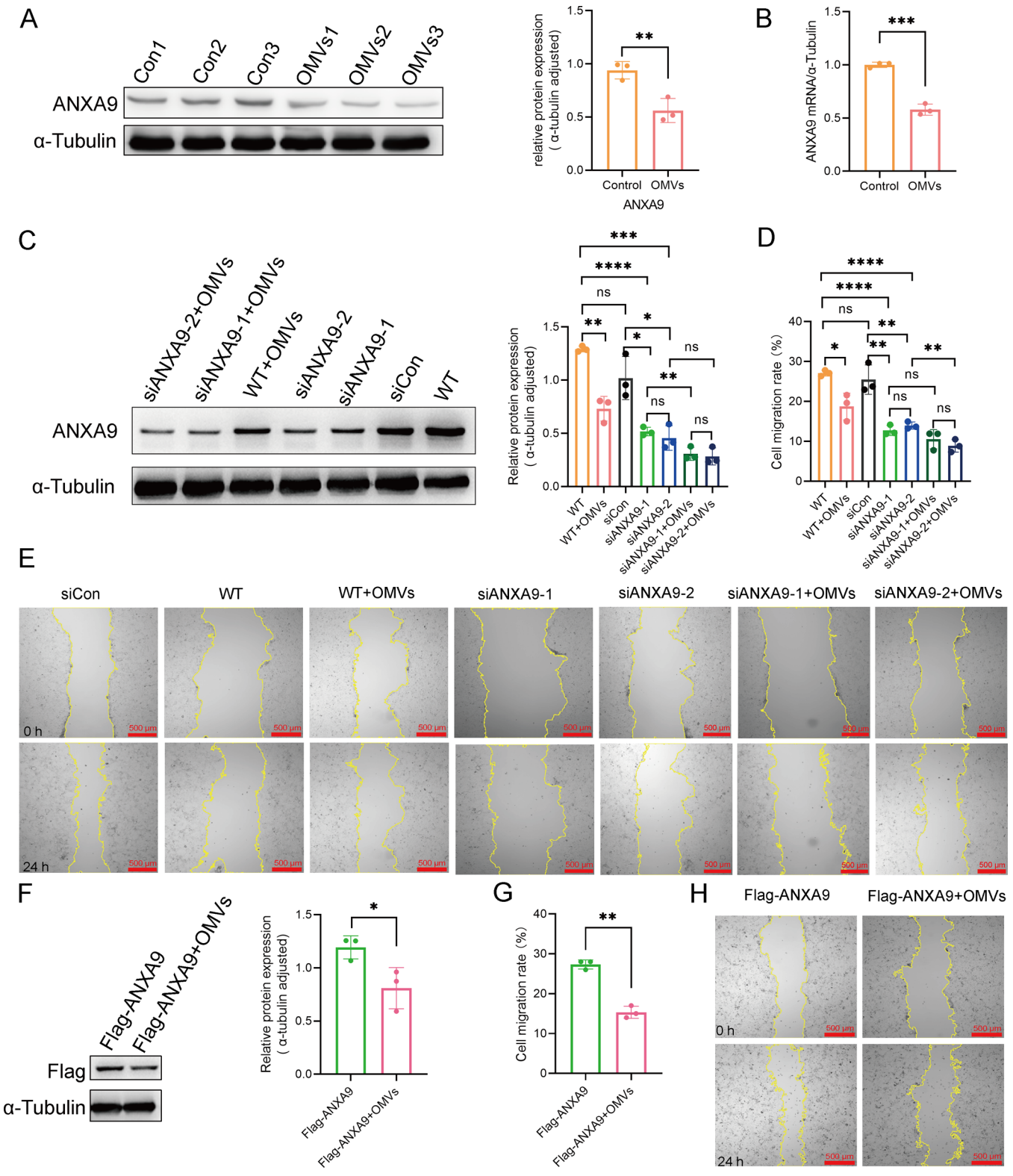

Figure 5. EcN 1917-derived OMVs inhibit cell migration by downregulating ANXA9. (A) Western blot and (B) qRT-PCR analysis showing downregulation of ANXA9 at protein and mRNA levels in Caco-2 cells after treatment with 10 μg/mL of OMVs for 24 h (n = 3). (C) Western blot showing the efficacy of ANXA9 knockdown in Caco-2 cells. The cells were silenced using siANXA9−1 and siANXA9−2 and then treated with OMVs. (D) bar graph and (E) cell scratch image showing cell migration after ANXA9 knockdown and OMV treatment. (F) Western blot showing the overexpression of ANXA9 in Caco-2 cells after treatment with 10 μg/mL OMVs for 24 h (n = 3). The cells were overexpressed with pcDNA3.1-Flag-ANXA9 plasmid, and OMVs were added (n = 3). (G) Bar graph and (H) cell scratch image showing the cell migration. The confluent monolayer of cells was scratched, and the cell migration area was measured 24 h later. Three biological replicates were performed. Unpaired two-tailed Student's t test. *p < 0.05, **p < 0.01. Mean ± SD.

https://doi.org/10.1021/acs.jproteome.4c00176
J. Proteome Res. XXXX, XXX, XXX−XXX

healing assay was performed to evaluate the effect of EcN 1917-derived OMVs on Caco-2 cell migration. The scratch area of premigrating cells was measured after treatment with OMVs, and after 24 h, the scratch area of cells postmigration was measured again.[29] A decreased scratch area was observed in the OMV-treated group, indicating the inhibitory effect of EcN 1917-derived OMVs on cell migration (Figure 3C, 3D). Third, an FD4 assay in a Transwell system was performed to investigate the influence of OMV treatment on the barrier permeability of Caco-2 cells.[20] Limited FD4 permeability in cells means that cell barrier integrity is maintained. The level of permeable FD4 in the OMV-treated group was significantly decreased, indicating that EcN 1917-derived OMVs inhibited cell permeability (Figure 3E). This result suggested that EcN 1917-derived OMVs contribute to maintaining the functional integrity of the epithelial barrier. Therefore, EcN 1917-derived OMVs can alter multiple cellular phenotypes in host cells.

Proteomic Profiles in Host Cells Are Altered by EcN 1917-Derived OMVs

To obtain molecular insight into the signaling pathways and underlying mechanisms by which EcN 1917-derived OMVs exert their effects, a quantitative proteomics experiment was performed by comparative analysis of OMV-free and OMV-treated Caco-2 cells. A Pearson correlation greater than 0.9 (Figure 4A) indicated high-quality reproducibility. PCA revealed that the OMV-treated group was separated from the OMV-free group (Figure 4B), indicating that a 24-h treatment with EcN 1917-derived OMVs caused a dramatic change in the proteomic architecture of Caco-2 cells. Further heatmaps and volcano plots revealed differentially expressed proteins induced by OMV treatment (Figure 4C, 4D, Data file S3), including 31 proteins with decreased abundance and 41 proteins with increased abundance. GO enrichment analysis indicated that these differentially expressed proteins were mainly enriched in biological processes such as lipid metabolism, protein trimerization, and stabilization; were localized in the cytoplasm and at cell−cell junctions; and exhibited molecular functions such as ATP binding and protein binding. (Figure 4E). Furthermore, KEGG pathway analysis revealed that these differentially expressed proteins are involved mainly in biological pathways such as the mRNA surveillance pathway, nucleocytoplasmic transport, and digestion and absorption of vitamins (Figure 4F). MCODE analysis of the protein−protein interaction network using the STRING database revealed that the clusters with the highest scores were related to protein binding (Figure 4G). Further network analysis using IPA software revealed clusters related to lipid metabolism, gene expression and the cell cycle (Figure 4H). According to the quantitative proteomics data, ANXA9 in host cells was downregulated by treatment with EcN 1917-derived OMVs (Figure 4I).

Among these differentially expressed proteins upon OMV treatment, ANXA9 and ST14 were reported to be associated with cancer cell migration.[30,31] ANXA9 belongs to the annexin family and is upregulated in various cancers, such as colorectal and gastric cancers.[30,32] It is primarily involved in the organization and regulation of the cell membrane and cytoskeletal connections, thereby impacting cell migration.[33] On the other hand, ST14 has been reported to only play roles in cell adhesion and basement membrane attachment.[31,34] Herein, ANXA9 was subjected to further functional validation.

EcN 1917-Derived OMVs Inhibit Host Cell Migration by Downregulating ANXA9

The MS-based ANXA9 data were further validated by Western blotting and qRT−PCR, and ANXA9 expression at both the protein and mRNA levels in Caco-2 cell decreased upon treatment with EcN 1917-derived OMVs (Figure 5A, 5B). Furthermore, EcN 1917-derived OMV treatment also inhibited cell migration and ANXA9 expression in NCM 460 cells (Figure S3). ANXA9 has been reported to be overexpressed in the biopsies of patients who develop colorectal cancer, and the overexpression of ANXA9 in cultured cells promoted cell migration.[30] Therefore, we speculated that ANXA9 may play a role in the OMV-mediated inhibition of cell migration. To confirm this possibility, we conducted a wound healing assay using an ANXA9-knockdown cell line. Specifically, Caco-2 cells were silenced with two pairs of siRNAs (siANXA9−1 and siANXA9−2) to prevent off-target effects. Western blotting revealed that ANXA9 protein expression was suppressed by ANXA9 knockdown (Figure 5C). Then, Caco-2 cells transfected with siRNA were allowed to form a monolayer and treated with EcN 1917-derived OMVs, after which the premigration and postmigration scratch areas were measured to calculate the cell migration rate. As a control, treating WT cells with OMVs inhibited cell migration (Figure 5D,5E). Knockdown of the ANXA9 protein by either siANXA9−1 or siANXA9−2 inhibited cell migration, and subsequently, treatment of these ANXA9-knockdown cell lines with OMVs promoted this inhibitory effect (Figure 5D,5E). Furthermore, ANXA9 was overexpressed by transfecting the recombinant plasmid pcDNA3.1-Flag-ANXA9 into Caco-2 cells, and as expected, subsequently treating these ANXA9-overexpressing cell lines with EcN 1917-derived OMVs suppressed the expression of the ANXA9 protein (Figure 5F). Wound healing experiments were further performed using these ANXA9-overexpressing cell lines. Compared with that in the WT group, cell migration was promoted in the ANXA9-overexpressing group, and subsequently, treating the ANXA9-overexpressing cells with OMVs inhibited cell migration (Figure 5G, 5H). Taken together, these results clearly indicate that EcN 1917-derived OMVs inhibited host cell migration by downregulating the mRNA and protein expression of ANXA9.

Alterations in the Phosphoproteomic Profiles of Host Cells Caused by EcN 1917-Derived OMVs

Protein phosphorylation in cells is sensitive to external or internal perturbations, and many previous reports have shown that kinase signaling pathways are critical for the regulation of cell migration. Therefore, we performed a quantitative phosphoproteomic analysis of Caco-2 cells disrupted by EcN 1917-derived OMVs to explore the possible molecular mechanisms involved. Because the internalization of OMVs into host cells occurs slowly and becomes significant at 24 h,[35] this time point of OMV incubation was used to monitor phosphoproteomic changes in host cells. The Pearson correlation coefficient of the quantitative data from the three biological replicates was >0.9, indicating reliable reproducibility (Figure S1A). We analyzed the distribution of all phosphorylation sites and found that 76% of phosphoproteins had multiple (i.e., 2 or more) phosphorylation sites (Figure S1B). In total, 5081 phosphorylation sites were identified, most of which were serine (85%), threonine (14%), and tyrosine (1%) (Figure S1C). PCA revealed that phosphorylation in the proteome of host cells changed after 24 h of treatment with

https://doi.org/10.1021/acs.jproteome.4c00176
J. Proteome Res. XXXX, XXX, XXX−XXX

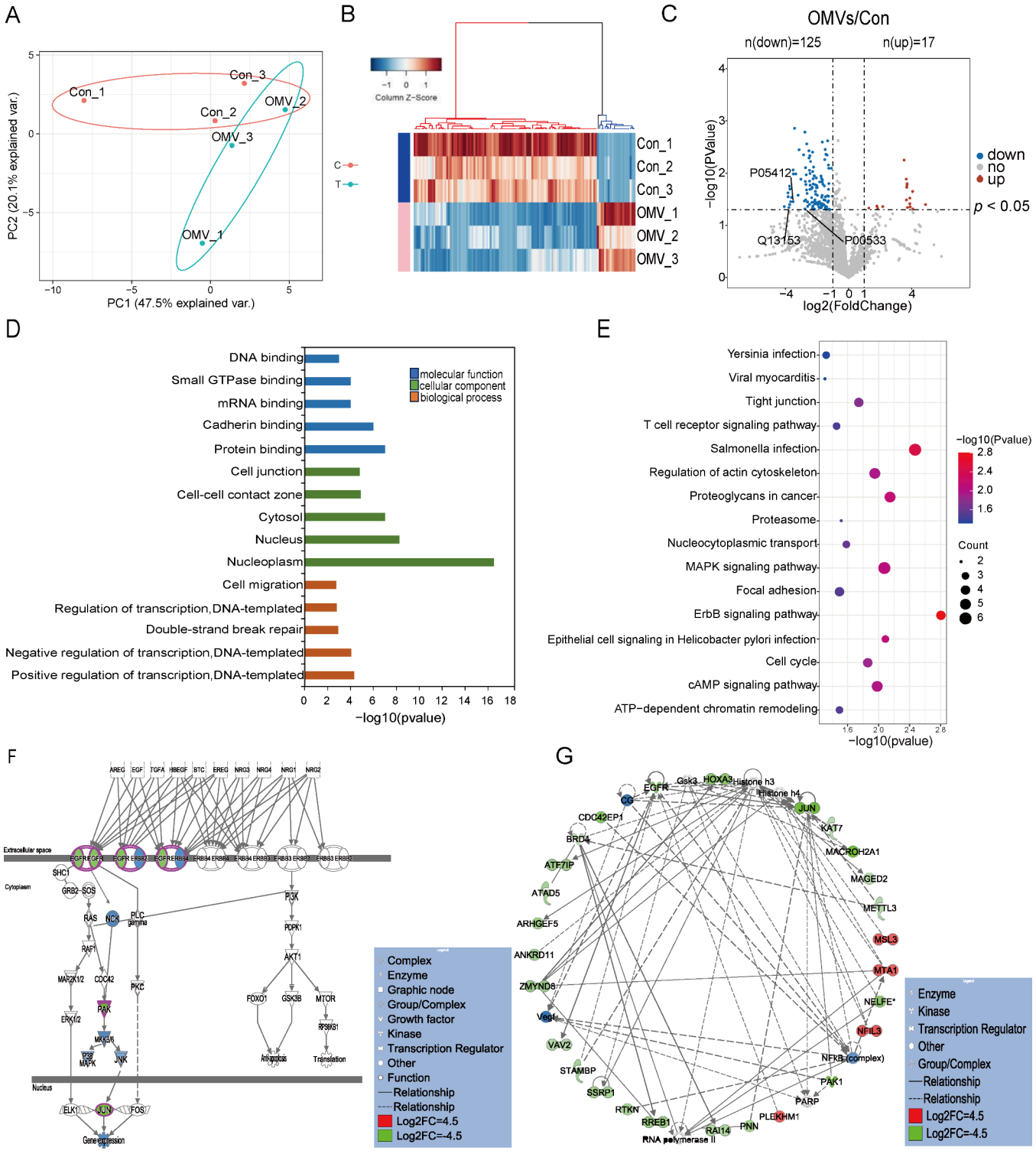

Figure 6. Phosphoproteomic analysis of Caco-2 cells perturbed by EcN 1917-derived OMVs. (A) PCA analysis of the identified phosphorylation sites in OMV-treated cells (OMV) and OMV-free cells (Con). Three biological replicates were performed. (B) Heat map and (C) volcano plot of differentially expressed phosphorylation sites in OMV-treated cells compared to OMV-free cells. Differentially expressed phosphorylation sites are determined by fold change >2 or <0.5 and $p < 0.05$. (D) GO and (E) KEGG analysis of differentially expressed phosphoproteins. GO, $p < 0.05$. KEGG, $p < 0.01$. (F) Pathway analysis of differentially expressed phosphoproteins showing the ErbB pathway. (G) Protein−protein interaction network analysis. Those were performed using IPA.

OMVs, as evidenced by the partial separation of the OMV-treated and OMV-free groups (Figure 6A). A heatmap and volcano plot revealed differentially expressed phosphorylation sites induced by OMV treatment (Figure 6B, 6C, Data File S4), including 17 upregulated sites and 125 downregulated sites. The enriched motif of the downregulated phosphorylated sites was [xPx_S_Px], that of the upregulated sites was [x_S_Px] (Figure S1D). GO analysis of the differentially

https://doi.org/10.1021/acs.jproteome.4c00176
J. Proteome Res. XXXX, XXX, XXX−XXX

expressed phosphorylated proteins revealed that the top 5 enriched terms included molecular functions such as protein binding, mRNA binding, and small GTPase binding, as well as biological processes such as the positive or negative control of DNA-template transcription, cell migration, and double-strand break repair (Figure 6D). KEGG analysis revealed that the pathways involved in the regulation of cell migration were the most enriched in the ErbB, MAPK and cAMP pathways, and the ErbB pathway was the most enriched pathway (Figure 6E). Network analysis using the STRING database revealed that the top-scoring clusters were related to DNA replication and the cell cycle (Figure S1E). Furthermore, functional domain analysis revealed the top-ranked domains, including coiled-coil, PDZ and transmembrane domains, PDZ domain and transmembrane domain (Figure S2). Remarkably, further analysis using IPA software (Figure 6F, 6G) revealed that the ErbB pathway was highly enriched, and phosphorylation of EGFR activated JUN through PAK1 to mediate cell migration.[36,37] Therefore, phosphoproteomic data revealed dramatic changes in functional phosphoproteins and related kinase signaling pathways perturbed by OMV treatment, and many of these proteins were enriched in the regulation of cell migration.

DISCUSSION

EcN 1917 is a nonpathogenic, Gram-negative strain that effectively colonizes tumor tissues and has shown promise for use in cancer therapy.[38] To understand the underlying mechanism of the interaction between EcN 1917 and host cells via OMV-mediated communication, we evaluated the phenotypic effects of EcN 1917-derived OMVs on host cells and constructed proteomic maps of the EcN 1917-derived OMV components and OMV-perturbed host cells. The number of proteins identified in our EcN 1917-derived OMV proteome was approximately four times greater than that previously reported. OMV treatment altered the proteomic and phosphoproteomic profiles of host cells. Importantly, for the first time, we found that OMV treatment could inhibit cancer cell migration by downregulating the protein expression of ANXA9.

Bacterial OMVs carry multiple cargos, of which proteins are the major components and are crucial for the function of OMVs.[39] Previous studies have shown that proteins isolated from probiotic-derived OMVs exhibit biological activities similar to those of intact OMVs.[27] Our proteomic results revealed that EcN 1917-derived OMVs carry a substantial amount of functionally important proteins that not only participate in bacterial regulation but also contribute to bacterial interactions with the host. For instance, flagellin, specifically FlgK and FlgE, can stimulate Toll-like receptor 5 and are closely associated with the biogenesis of EcN 1917 biofilms and intestinal colonization.[40] Transaldolase exhibits high adhesive ability and serves as a colonization factor on host cells.[41] Enolase plays a role in molecular communication between *Bifidobacterium lactis* and the human host through plasminogen, which binds to the K251, K255 and Glu252 residues of enolase.[42] Our results indicate that EcN 1917-released OMVs can be internalized by host cells, which might offer favorable conditions for these proteins to interact with host cells. Therefore, our results offer a valuable data resource for further investigations of bacteria−host interactions via OMV communication.

Our results also showed that EcN 1917-derived OMVs can affect various phenotypes of host cells, particularly by inhibiting cell migration. Furthermore, OMV treatment significantly altered the protein profile and phosphorylation network in Caco-2 cells. Many differentially expressed proteins were enriched in cell−cell junctions, suggesting the involvement of OMVs in intracellular and intercellular communication and structural organization. Furthermore, nucleocytoplasmic transport, which is involved in the regulation of macromolecule transport, such as protein and mRNA transport, was enriched between the nucleus and cytoplasm, suggesting potential crosstalk between OMVs and host cells. Bioinformatic analysis of the phosphoproteome indicated that OMV treatment influenced signaling pathways related to cell migration, such as ErbB, MAPK, and cAMP, suggesting that these pathways may play roles in the regulation of OMV-mediated cell migration. Among them, EGFR, PAK1, and JUN are key proteins in the ErbB pathway, and previous studies have shown that PAK1 plays a role in cancer progression.[43] Decreased PAK1 expression can reduce cell proliferation and migration/invasion and inhibit the development of colorectal cancer.[44] Our data show that OMV-induced phosphorylation of EGFR/PAK1/JUN is reduced; thus, ErbB may be one of the potential pathways leading to the inhibition of cell migration.

ANXA9, a member of the annexin family, contains four internal repeated structural domains, each of which includes a type II calcium-binding site and is essential for interacting with membrane phospholipids. Previous research has suggested that ANXA9 expression is associated with bone metastasis in breast cancer and may impact cell growth, migration, and epithelial−mesenchymal transition through the TGF-β signaling pathway.[45] Yu et al.[30] reported that ANXA9 promoted the invasion and metastasis of colorectal cancer, and ANXA9 overexpression predicted poor patient prognosis. In our study, knocking down ANXA9 protein inhibited cell migration, and this inhibitory effect was further enhanced by treatment with EcN 1917-derived OMVs. Furthermore, ANXA9-overexpressing cells tended to exhibit enhanced cell migration, but treatment with OMVs reversed the simulative effect on cell migration. Therefore, EcN 1917-derived OMVs suppressed the migration of Caco-2 cells by downregulating the expression of ANXA9. It is speculated that OMVs could influence the expression of ANXA9 within cells through molecular signals such as proteins or RNA, thereby modulating intracellular signaling pathways. This worths a further in-depth investigation.

CONCLUSIONS

This study is the first to demonstrate that EcN 1917-derived OMVs mediate host cell migration. Proteomic analysis of EcN 1917-derived OMVs greatly extended the available data on OMV protein cargos and revealed diverse functionally important proteins, as well as many proteins involved in bacteria−host interactions. Perturbation using EcN 1917-derived OMVs altered the architectures of the proteome and phosphoproteome in host cells. OMVs derived from EcN 1917 inhibited host cell migration by downregulating the mRNA and protein expression of ANXA9. In addition, phosphoproteomic data suggested that the ErbB pathway may be involved in OMV-mediated cell migration. Overall, our study provides valuable data for further investigations of OMV-mediated bacteria−host interactions and offers great insights into the

https://doi.org/10.1021/acs.jproteome.4c00176
J. Proteome Res. XXXX, XXX, XXX−XXX

underlying mechanism of probiotic-assisted colorectal cancer therapy.

■ ASSOCIATED CONTENT

Data Availability Statement

The mass spectrometry proteomics data have been deposited to the ProteomeXchange Consortium through the iProX partner repository[46] with the data set identifier PXD050386.

Supporting Information

The Supporting Information is available free of charge at https://pubs.acs.org/doi/10.1021/acs.jproteome.4c00176.

Figure S1. Phosphoproteomic analysis of Caco-2 cells; Figure S2. Functional domain analysis; Figure S3. The cell migration and ANXA9 protein expression; Figure S4. Entire membrane image of Western blot; Table S1. Primers used in this study; Table S2. siRNAs used in this study (PDF)

Data file S1. The identified OMV cargo proteins (XLSX)

Data file S2. The identified top 100 abundant OMV proteins (XLSX)

Data file S3. The differentially expressed proteins in Caco-2 cells (XLSX)

Data file S4. The differentially expressed phosphorylated sites in Caco-2 cells (XLSX)

Data file S5. The peptides for motif analysis (XLSX)

■ AUTHOR INFORMATION

Corresponding Authors

Xiankun Wang − *National Center for Protein Sciences − Beijing, Beijing Proteome Research Center, State Key Laboratory of Medical Proteomics, Beijing Institute of Lifeomics, Beijing 102206, China;* orcid.org/0000-0003-2004-4927; Email: wangxiankun@ncpsb.org.cn

Chenxi Jia − *School of Basic Medical Sciences, Anhui Medical University, Hefei, Anhui 230032, China; National Center for Protein Sciences − Beijing, Beijing Proteome Research Center, State Key Laboratory of Medical Proteomics, Beijing Institute of Lifeomics, Beijing 102206, China;* orcid.org/0000-0001-6334-5282; Email: cjia@ncpsb.org.cn

Authors

Ling Zhao − *School of Basic Medical Sciences, Anhui Medical University, Hefei, Anhui 230032, China; National Center for Protein Sciences − Beijing, Beijing Proteome Research Center, State Key Laboratory of Medical Proteomics, Beijing Institute of Lifeomics, Beijing 102206, China*

Mingxin Zhao − *National Center for Protein Sciences − Beijing, Beijing Proteome Research Center, State Key Laboratory of Medical Proteomics, Beijing Institute of Lifeomics, Beijing 102206, China*

Complete contact information is available at: https://pubs.acs.org/10.1021/acs.jproteome.4c00176

Author Contributions

CJ and XW designed the project. LZ and XW conducted the experiments and data analysis. LZ, XW, and CJ prepared the manuscript. CJ extensively revised the manuscript.

Notes

The authors declare no competing financial interest.

■ ACKNOWLEDGMENTS

This work is supported by the National Key R&D Program of China (No. 2023YFF0713804 and 2021YFA1302601 to CJ), National Science Foundation of China (no. 32300017 to XW) and the Foundation of State Key Laboratory (SKLP-O202203 to CJ). We thank the mass spectrometry facility of the Phoenix Center for accessing the instruments.

■ REFERENCES

(1) Schultz, M. Clinical use of E. coli Nissle 1917 in inflammatory bowel disease. *Inflamm Bowel Dis* **2008**, *14* (7), 1012−1018.

(2) Sanders, M. E.; Merenstein, D. J.; Reid, G.; Gibson, G. R.; Rastall, R. A. Probiotics and prebiotics in intestinal health and disease: from biology to the clinic. *Nat. Rev. Gastroenterol Hepatol* **2019**, *16* (10), 605−616.

(3) Kim, S. K.; Guevarra, R. B.; Kim, Y. T.; Kwon, J.; Kim, H.; Cho, J. H.; Kim, H. B.; Lee, J. H. Role of Probiotics in Human Gut Microbiome-Associated Diseases. *J. Microbiol Biotechnol* **2019**, *29* (9), 1335−1340.

(4) Tomasi, M.; Caproni, E.; Benedet, M.; Zanella, I.; Giorgetta, S.; Dalsass, M.; König, E.; Gagliardi, A.; Fantappiè, L.; Berti, A.; et al. Outer Membrane Vesicles From The Gut Microbiome Contribute to Tumor Immunity by Eliciting Cross-Reactive T Cells. *Front Oncol* **2022**, *12*, 912639.

(5) Sonnenborn, U. Escherichia coli strain Nissle 1917-from bench to bedside and back: history of a special Escherichia coli strain with probiotic properties. *FEMS Microbiol. Lett.* **2016**, *363* (19), fnw212.

(6) Secher, T.; Kassem, S.; Benamar, M.; Bernard, I.; Boury, M.; Barreau, F.; Oswald, E.; Saoudi, A. Oral Administration of the Probiotic Strain Escherichia coli Nissle 1917 Reduces Susceptibility to Neuroinflammation and Repairs Experimental Autoimmune Encephalomyelitis-Induced Intestinal Barrier Dysfunction. *Front. Immunol.* **2017**, *8*, 1096.

(7) Scaldaferri, F.; Gerardi, V.; Mangiola, F.; Lopetuso, L. R.; Pizzoferrato, M.; Petito, V.; Papa, A.; Stojanovic, J.; Poscia, A.; Cammarota, G.; et al. Role and mechanisms of action of Escherichia coli Nissle 1917 in the maintenance of remission in ulcerative colitis patients: An update. *World J. Gastroenterol* **2016**, *22* (24), 5505−5511.

(8) Fábrega, M. J.; Aguilera, L.; Giménez, R.; Varela, E.; Alexandra Cañas, M.; Antolín, M.; Badía, J.; Baldomà, L. Activation of Immune and Defense Responses in the Intestinal Mucosa by Outer Membrane Vesicles of Commensal and Probiotic Escherichia coli Strains. *Front. Microbiol.* **2016**, *7*, 705.

(9) Alvarez, C. S.; Badia, J.; Bosch, M.; Giménez, R.; Baldomà, L. Outer Membrane Vesicles and Soluble Factors Released by Probiotic Escherichia coli Nissle 1917 and Commensal ECOR63 Enhance Barrier Function by Regulating Expression of Tight Junction Proteins in Intestinal Epithelial Cells. *Front. Microbiol.* **2016**, *7*, 1981.

(10) Yu, X.; Lin, C.; Yu, J.; Qi, Q.; Wang, Q. Bioengineered Escherichia coli Nissle 1917 for tumour-targeting therapy. *Microb Biotechnol* **2020**, *13* (3), 629−636.

(11) Jiang, L.; Shen, Y.; Guo, D.; Yang, D.; Liu, J.; Fei, X.; Yang, Y.; Zhang, B.; Lin, Z.; Yang, F.; et al. EpCAM-dependent extracellular vesicles from intestinal epithelial cells maintain intestinal tract immune balance. *Nat. Commun.* **2016**, *7*, 13045.

(12) Kulp, A.; Kuehn, M. J. Biological functions and biogenesis of secreted bacterial outer membrane vesicles. *Annu. Rev. Microbiol.* **2010**, *64*, 163−184.

(13) Kaparakis-Liaskos, M.; Ferrero, R. L. Immune modulation by bacterial outer membrane vesicles. *Nat. Rev. Immunol* **2015**, *15* (6), 375−387.

(14) Díaz-Garrido, N.; Badia, J.; Baldomà, L. Microbiota-derived extracellular vesicles in interkingdom communication in the gut. *J. Extracell. Vesicles* **2021**, *10* (13), e12161.

(15) Kim, O. Y.; Park, H. T.; Dinh, N. T. H.; Choi, S. J.; Lee, J.; Kim, J. H.; Lee, S. W.; Gho, Y. S. Bacterial outer membrane vesicles

suppress tumor by interferon-γ-mediated antitumor response. *Nat. Commun.* **2017**, *8* (1), 626.
(16) Acevedo, R.; Fernández, S.; Zayas, C.; Acosta, A.; Sarmiento, M. E.; Ferro, V. A.; Rosenqvist, E.; Campa, C.; Cardoso, D.; Garcia, L.; et al. Bacterial outer membrane vesicles and vaccine applications. *Front. Immunol.* **2014**, *5*, 121.
(17) Aly, R. G.; El-Enbaawy, M. I.; Abd El-Rahman, S. S.; Ata, N. S. Antineoplastic activity of Salmonella Typhimurium outer membrane nanovesicles. *Exp. Cell Res.* **2021**, *399* (1), 112423.
(18) Praveschotinunt, P.; Duraj-Thatte, A. M.; Gelfat, I.; Bahl, F.; Chou, D. B.; Joshi, N. S. Engineered E. coli Nissle 1917 for the delivery of matrix-tethered therapeutic domains to the gut. *Nat. Commun.* **2019**, *10* (1), 5580.
(19) Aguilera, L.; Toloza, L.; Giménez, R.; Odena, A.; Oliveira, E.; Aguilar, J.; Badia, J.; Baldomà, L. Proteomic analysis of outer membrane vesicles from the probiotic strain Escherichia coli Nissle 1917. *Proteomics* **2014**, *14* (2−3), 222−229.
(20) Wei, S.; Zhang, J.; Wu, X.; Chen, M.; Huang, H.; Zeng, S.; Xiang, Z.; Li, X.; Dong, W. Fusobacterium nucleatum Extracellular Vesicles Promote Experimental Colitis by Modulating Autophagy via the miR-574−5p/CARD3 Axis. *Inflamm Bowel Dis* **2023**, *29* (1), 9−26.
(21) Wiśniewski, J. R.; Zougman, A.; Nagaraj, N.; Mann, M. Universal sample preparation method for proteome analysis. *Nat. Methods* **2009**, *6* (5), 359−362.
(22) Rappsilber, J.; Mann, M.; Ishihama, Y. Protocol for micro-purification, enrichment, pre-fractionation and storage of peptides for proteomics using StageTips. *Nat. Protoc* **2007**, *2* (8), 1896−1906.
(23) Cox, J.; Mann, M. MaxQuant enables high peptide identification rates, individualized p.p.b.-range mass accuracies and proteome-wide protein quantification. *Nat. Biotechnol.* **2008**, *26* (12), 1367−1372.
(24) Sherman, B. T.; Hao, M.; Qiu, J.; Jiao, X.; Baseler, M. W.; Lane, H. C.; Imamichi, T.; Chang, W. DAVID: a web server for functional enrichment analysis and functional annotation of gene lists (2021 update). *Nucleic Acids Res.* **2022**, *50* (W1), W216−W221.
(25) Letunic, I.; Khedkar, S.; Bork, P. SMART: recent updates, new developments and status in 2020. *Nucleic Acids Res.* **2021**, *49* (D1), D458−D460.
(26) Wang, S.; Cai, Y.; Cheng, J.; Li, W.; Liu, Y.; Yang, H. motifeR: An Integrated Web Software for Identification and Visualization of Protein Posttranslational Modification Motifs. *Proteomics* **2019**, *19* (23), e1900245.
(27) Hu, R.; Lin, H.; Li, J.; Zhao, Y.; Wang, M.; Sun, X.; Min, Y.; Gao, Y.; Yang, M. Probiotic Escherichia coli Nissle 1917-derived outer membrane vesicles enhance immunomodulation and antimicrobial activity in RAW264.7 macrophages. *BMC Microbiol.* **2020**, *20* (1), 268.
(28) Bian, B.; Zhao, C.; He, X.; Gong, Y.; Ren, C.; Ge, L.; Zeng, Y.; Li, Q.; Chen, M.; Weng, C.; et al. Exosomes derived from neural progenitor cells preserve photoreceptors during retinal degeneration by inactivating microglia. *J. Extracell. Vesicles* **2020**, *9* (1), 1748931.
(29) Bae, I. H.; Park, D. S.; Lee, S. Y.; Jang, E. J.; Shim, J. W.; Lim, K. S.; Park, J. K.; Kim, J. H.; Sim, D. S.; Jeong, M. H. Bilirubin coating attenuates the inflammatory response to everolimus-coated stents. *J. Biomed Mater. Res. B Appl. Biomater* **2018**, *106* (4), 1486−1495.
(30) Yu, S.; Bian, H.; Gao, X.; Gui, L. Annexin A9 promotes invasion and metastasis of colorectal cancer and predicts poor prognosis. *Int. J. Mol. Med.* **2018**, *41* (4), 2185−2192.
(31) Ding, K. F.; Sun, L. F.; Ge, W. T.; Hu, H. G.; Zhang, S. Z.; Zheng, S. Effect of SNC19/ST14 gene overexpression on invasion of colorectal cancer cells. *World J. Gastroenterol* **2005**, *11* (36), 5651−5654.
(32) Zhang, T.; Yu, S.; Zhao, S. ANXA9 as a novel prognostic biomarker associated with immune infiltrates in gastric cancer. *PeerJ.* **2021**, *9*, e12605.
(33) Lu, C.; Zhan, Y.; Jiang, Y.; Liao, J.; Qiu, Z. Exosome-derived ANXA9 functions as an oncogene in breast cancer. *J. Pathol Clin Res.* **2023**, *9* (5), 378−390.
(34) Sun, L. F.; Zheng, S.; Shi, Y.; Fang, X. M.; Ge, W. T.; Ding, K. F. [SNC19/ST14 gene transfection and expression influence the biological behavior of colorectal cancer cells]. *Zhonghua Yi Xue Za Zhi* **2004**, *84* (10), 843−848.
(35) Ling, Z.; Dayong, C.; Denggao, Y.; Yiting, W.; Liaoqiong, F.; Zhibiao, W. Escherichia Coli Outer Membrane Vesicles Induced DNA Double-Strand Breaks in Intestinal Epithelial Caco-2 Cells. *Med. Sci. Monit Basic Res.* **2019**, *25*, 45−52.
(36) Howe, A. K. Cell adhesion regulates the interaction between Nck and p21-activated kinase. *J. Biol. Chem.* **2001**, *276* (18), 14541−14544.
(37) Li, X.; Li, F. p21-Activated Kinase: Role in Gastrointestinal Cancer and Beyond. *Cancers* **2022**, *14* (19), 4736.
(38) Stritzker, J.; Weibel, S.; Hill, P. J.; Oelschlaeger, T. A.; Goebel, W.; Szalay, A. A. Tumor-specific colonization, tissue distribution, and gene induction by probiotic Escherichia coli Nissle 1917 in live mice. *Int. J. Med. Microbiol* **2007**, *297* (3), 151−162.
(39) Brown, L.; Wolf, J. M.; Prados-Rosales, R.; Casadevall, A. Through the wall: extracellular vesicles in Gram-positive bacteria, mycobacteria and fungi. *Nat. Rev. Microbiol* **2015**, *13* (10), 620−630.
(40) Choi, D. S.; Kim, D. K.; Choi, S. J.; Lee, J.; Choi, J. P.; Rho, S.; Park, S. H.; Kim, Y. K.; Hwang, D.; Gho, Y. S. Proteomic analysis of outer membrane vesicles derived from Pseudomonas aeruginosa. *Proteomics* **2011**, *11* (16), 3424−3429.
(41) González-Rodríguez, I.; Sánchez, B.; Ruiz, L.; Turroni, F.; Ventura, M.; Ruas-Madiedo, P.; Gueimonde, M.; Margolles, A. Role of extracellular transaldolase from Bifidobacterium bifidum in mucin adhesion and aggregation. *Appl. Environ. Microbiol.* **2012**, *78* (11), 3992−3998.
(42) Candela, M.; Biagi, E.; Centanni, M.; Turroni, S.; Vici, M.; Musiani, F.; Vitali, B.; Bergmann, S.; Hammerschmidt, S.; Brigidi, P. Bifidobacterial enolase, a cell surface receptor for human plasminogen involved in the interaction with the host. *Microbiology* **2009**, *155* (10), 3294−3303.
(43) Ye, D. Z.; Field, J. PAK signaling in cancer. *Cell Logist* **2012**, *2* (2), 105−116.
(44) Huynh, N.; Liu, K. H.; Baldwin, G. S.; He, H. P21-activated kinase 1 stimulates colon cancer cell growth and migration/invasion via ERK- and AKT-dependent pathways. *Biochim. Biophys. Acta* **2010**, *1803* (9), 1106−1113.
(45) Zhou, Y.; Qiu, C.; Wang, T.; Tao, L.; Zhang, Z.; Yao, J. High Expression of Annexin A9 Promotes Cell Proliferation and Migration in Gastric Cancer via the TGF-β Signaling Pathway. *J. Environ. Pathol Toxicol Oncol* **2021**, *40* (3), 87−94.
(46) Ma, J.; Chen, T.; Wu, S.; Yang, C.; Bai, M.; Shu, K.; Li, K.; Zhang, G.; Jin, Z.; He, F.; et al. iProX: an integrated proteome resource. *Nucleic Acids Res.* **2019**, *47* (D1), D1211−D1217.

https://doi.org/10.1021/acs.jproteome.4c00176
J. Proteome Res. XXXX, XXX, XXX−XXX